ELSEVIER

Journal of Neuroscience Methods 77 (1997) 31–41

JOURNAL OF NEUROSCIENCE METHODS

Development of a narrow water-immersion objective for laserinterferometric and electrophysiological applications in cell biology

Hannes Maier [a,*], Christoph Zinn [a], Andreas Rothe [1,b], Hans Tiziani [b], Anthony W. Gummer [a]

[a] *Section of Physiological Acoustics and Communication, Department of Otolaryngology, University of Tübingen, Silcherstr. 5, D-72076 Tübingen, Germany*

[b] *Institut für Technische Optik, Stuttgart, Germany*

Received 5 November 1996; received in revised form 16 June 1997; accepted 20 June 1997

Abstract

Laserinterferometric studies of the micromechanical properties of the organ of Corti using isolated temporal bone preparations are well established. However, there are relatively few measurements under in vivo conditions in the apical region of the cochlea because of its inaccessibility with commonly used techniques. Recently, optical-design programs have become affordable and powerful, so that the development of an optimized optical system is within the budget of physiologists and biophysicists. We describe here the development of a long-range water-immersion objective. To circumvent anatomical constraints, it has a narrow conical tip of taper 22° and diameter 2.4 mm. It is a bright-field reflected-light illumination, achromatic objective with magnification of $25\times/\infty$, a working distance of 2.180 mm and a numerical aperture of 0.45. Chromatic errors are corrected at 546.1 and 632.8 nm, with emphasis on the latter wavelength which is used by the laser interferometer. The field curvature is relatively flat and a diffraction limitation (Strehl ratio better than 0.8) can be obtained in a field of 0.4 mm diameter. Using this objective, sound-induced vibrations of hair cells and Hensen cells could be recorded without placing a reflector on the target area. In addition, this objective was found to be diffraction-limited in the near infra-red (750–830 nm), with a slightly different working distance (2.186 mm), making it suitable for patch-clamp experiments using infra-red, differential interference contrast. © 1997 Elsevier Science B.V.

Keywords: Laser Doppler vibrometry; Water-immersion objective; Cochlear micromechanics; Patch-clamp; Differential interference contrast

1. Introduction

A major part of modern biological and physiological research involves the study of cellular mechanisms inside "living" tissue. When working with sections of tissue in which the cells of interest are located directly under a glass cover, optimal resolution can be obtained with conventional, high numerical aperture, oil-immersion objectives corrected for the cover glass. However, the resolution is severely reduced when using these oil-immersion objectives for focusing at depths more than several tenths of micrometers within the tissue; this is due to the difference in refractive indices of glass (1.515) and tissue (1.33–1.35). Under these circumstances, better results can be obtained with water-immersion objectives, which are available for working distances from several tenths of millimeters to several millimeters. Optically optimized long-range objectives of this kind allow sufficient space between the tissue and the objective for many experimental purposes (e.g. patch-clamping) and, in addition, their outer shape is often adapted to the in vitro or in situ situation. Examples of four commercially available water-immersion objectives are given in Fig. 1. However, for in vivo

* Corresponding authors. Tel.: +49 7071 2984158; fax: +49 7071 294174.

[1] Present address: Hensoldt AG, Wetzlar, Germany.

PII S0165-0270(97)00105-2

experiments the situation may be less than optimal because lateral access for recording electrodes, for example, is not possible or because optical access is hindered for anatomical reasons.

In our application, an objective is required for focusing the light from a laser Doppler vibrometer onto cellular structures in the cochlea. Although we (Gummer et al., 1996) were able to make successful vibration measurements in a temporal bone preparation of the cochlea using a commercially available objective (Zeiss Acroplan 40x/0.75 WPh2), in vivo vibration experiments proved impossible because, unlike the in vitro situation, it was not possible to remove sufficient overlying tissue to allow access with the Zeiss objective (Fig. 2A). The in vivo experiments, requiring the neuronal and systemic inputs to the inner ear to be left undisturbed, must be conducted with a much smaller ventral opening of the middle-ear cavity or bulla (Fig. 2). This paper describes the objective (Fig. 1C, Fig. 2B) that we designed for the in vivo vibration measurements, giving its theoretical and experimental performance.

Vibration measurements in the apical (low-frequency) region of the in vitro (Khanna et al., 1989; Ulfendahl et al., 1989) and in vivo (Khanna and Hao, 1996) cochlea have made use of long-range air-objectives in combination with a dipping cone. However, the dipping cone is not commercially available. Unfortunately, relevant structures can be discerned only occasionally when using commercially available water-immersion objectives. For vibration measurements, a long-range air-objective without a dipping cone requires a glass window at the interposed fluid-air interface. Generally, a decrease in the signal-to-noise ratio is produced by additional reflections and poor image quality due to the uncompensated change of the refractive index in the optical path. To compensate for a loss of image quality, the endolymphatic space must be opened and under normal in vivo conditions reflective beads must be placed on the vibrating surface (Cooper and Rhode, 1995). It is possible, however, to make vibration measurements of the highly reflecting lipid droplets of Hensen cells without introducing a reflector (Cooper and Rhode, 1996).

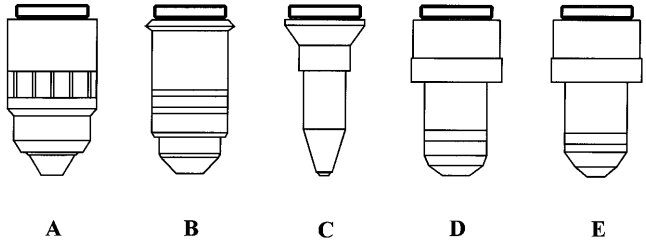

Fig. 1. Relative outer dimensions of five water-immersion objectives. A) Olympus WPlan 20 × /0.4 W 160/ − working distance WD = 3.1 mm. B) Olympus UMPlanFL 20 × /0.50 W ∞/0 WD = 3.3 mm. C) Our custom-built objective 25 × /0.45 W ∞/0 WD = 2.18 mm. D) Zeiss Achroplan 20 × /0.50 WPh2 ∞/0 WD = 1.97 mm. E) Zeiss Achroplan 40 × /0.75 WPh2 ∞/0 WD = 1.92 mm.

To design a dipping cone of high optical quality for a commercially built long-range objective, a knowledge of the detailed parameters of the objective is essential: Unfortunately, they are usually kept secret by the manufacturers. To avoid these disadvantages, we decided to develop a water-immersion objective with a narrow tip-diameter adapted to the special anatomical constraints of our experiments.

We present here an affordable way to develop and construct a custom-designed achromatic objective which is not only suited to our laser vibrometric experiments, but can also be used in other applications where space is a major constraint: for example, in certain types of patch-clamp experiment.

2. Specifications

Vibration measurements were to be made in the apical region of the cochlea by coupling the beam of a helium-neon (633 nm), laser Doppler vibrometer (Polytec OFV-302) into the side-arm of an epifluorescence microscope (Leitz Aristomet) (Fig. 3). This measurement technique has been used in vivo in the basal half of the cochlea (Ruggero and Rich, 1991; Nuttall et al., 1991) and in a temporal bone preparation in the apical half of the cochlea (Gummer et al., 1996).

Access to the apical end of the cochlea in vivo is limited anatomically, rendering commercially available water-immersion objectives unusable. However, these restrictions may be circumvented by an objective of conical shape, with an angle of less than 30°, a tip diameter of approximately 3 mm, and a working distance of 2.0–2.2 mm. Moreover, since vibration measurements and visual observation must be made from the same side, the object illumination is required *from the microscope side* (bright-field reflected-light illumination). In this application, therefore, reflections must be minimized in *both* the incident and the reflected pathways. This is especially important for the laser wavelength of 632.8 nm, because even small amounts of back-reflected light from surfaces inside the objective may decrease the effective sensitivity of the vibrometer. A broadband antireflection coating with $r < 0.5\%$, in combination with the appropriate geometry, will be shown to yield a sufficient and economical result.

A water-immersion objective is necessary to achieve optimal image quality and minimal reflections at intermediate fluid surfaces. Since the exact refractive index for the cochlear fluid was not available, the wavelength-dependent refractive index of isotonic NaCl solution was taken as a good approximation to the optical properties.

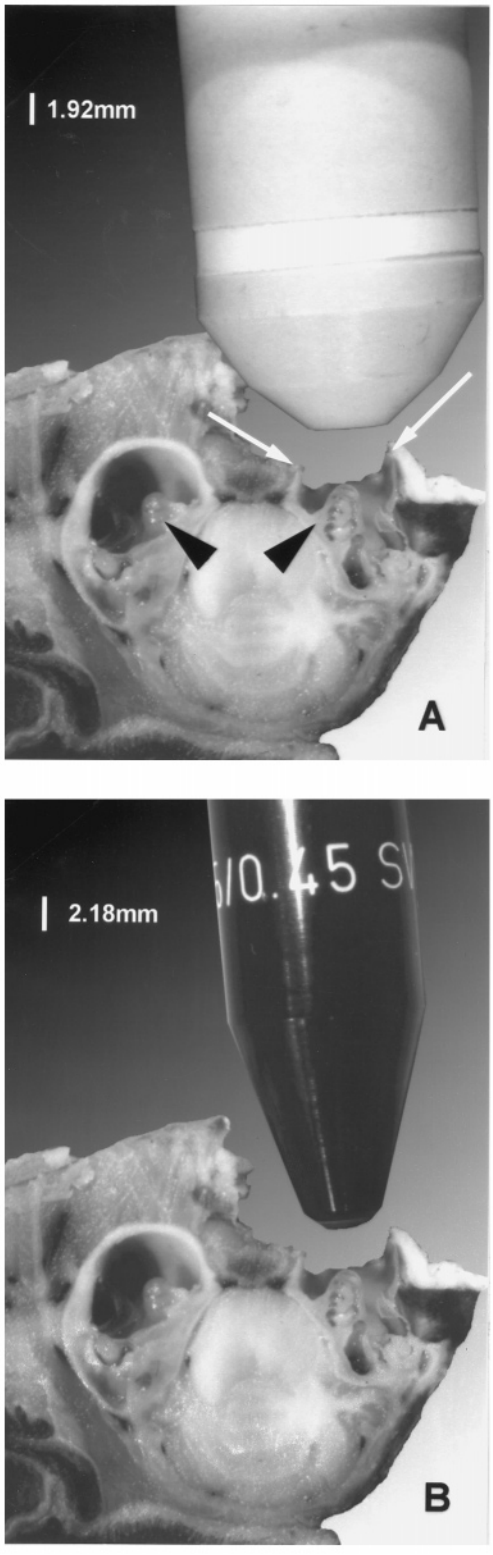

Fig. 2.

The long-working range and the diameter of the front lens restrict the attainable numerical aperture to not more than 0.45. Nevertheless, this was considered sufficient for our purposes.

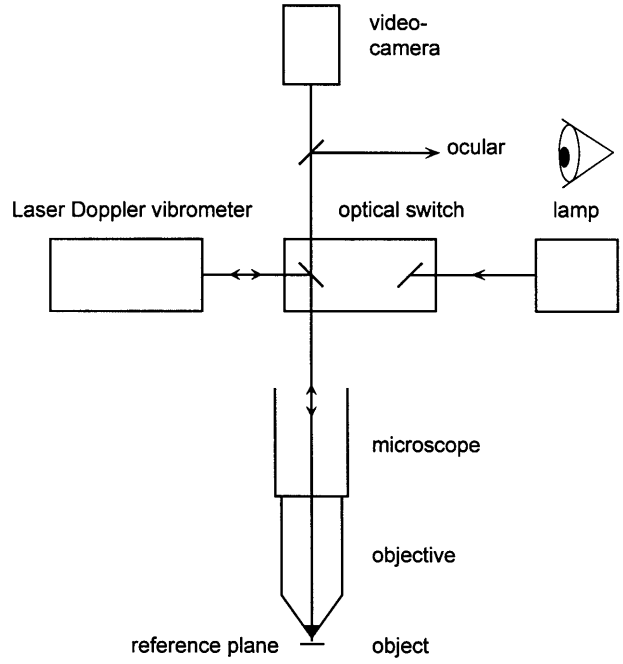

Fig. 3. Scheme of the laser-Doppler-vibrometer setup. The optical switch is used to choose between bright-field illumination and the bidirectional laser beam of the Doppler vibrometer.

The circumstances of the surgical approach make it impossible to change the objective (and magnification) during the experiment. Therefore, a comprimise magnification of approximately 25 was chosen, allowing resolution of relevant structures and coarse orientation by the experimenter. The need to orientate in three dimensions within the cochlea requires the broadest region of highest resolution in the center of the image. A region of diameter approximately 0.25 mm was deemed acceptable and technically feasible. This constraint led to two distinct requirements. Firstly, in the central field the sharp image should lie on the plane perpendicular to the optical axis (this is equivalent to a flat field and the absence of astigmatism). Flat-field microscope objectives usually incorporate the letters 'plan' in some form in their commercial brand names. Secondly, the objective should be diffraction-limited. Quantitatively, this is equivalent to the requirement

Fig. 2. Relative sizes of objectives demonstrated with a section through the cranial bone and cochlea. A: Zeiss Achroplan 40 × /0.75 WPh2 long-range water-immersion objective with a working distance of 1.92 mm. B: the designed objective demonstrating the accessibility to the apical region of the cochlea. The opening of the bulla is restricted by the tympanic membrane (right, white arrow) and the skull base (left, white arrow). In the left side of each picture the cochlea (left, black arrowhead) is intact, whereas on the right side it has been cut longitudinally (right, black arrowhead). Note that large amounts of bone and tissue have been removed solely for the purpose of illustration. Working distances for each objective are indicated by bars.

that the Strehl ratio be better than 0.8. The Strehl ratio is just the intensity at the center of the image of a point light source for an aberrated system expressed as a fraction of the corresponding intensity for a perfect (aberration free) system (Smith, 1990; Hilger, 1996).

In order to reduce chromatic errors, the diffraction limitation requirement should be satisfied at two wavelengths. With two wavelengths the effort for the numerical calculation and the mechanical construction were within the limits of our possibilities and were affordable. Normally, this type of 'achromatic objective' is corrected for red and blue light. Apochromats, which are corrected for three wavelengths, would have increased the manufacturing costs by at least a factor of four to five. For a minimum quantity of ten pieces of custom-built objectives fitting these requirements, the production costs were less than US$800 each.

3. Methods

3.1. Design and numerical optimization

The performance of the optical system was determined and optimized using two different optical design programs: Code V (Optical Research Associates, CA, USA) and ZEMAX (Optima Research Ltd., UK). Although these programs are highly elaborate, it must be emphasized that the success of a lens' design depends strongly on the quality of the initial estimates of the lens' parameters. The design of an objective from a zero starting point requires much more experience than was available in our group. Our initial estimates were provided by the manufacturer (Syncotec, Wetzlar, Germany), who is experienced in constructing air-objectives with an outer shape similar to our requirements. Patented data, which can be used legally for scientific purposes, would have also provided adequate initial estimates. From this starting point, numerical optimization under the given restrictions was performed using built-in standard routines of the above mentioned programs. The restrictions concerning the distances and diameters of the first two double lenses were especially important because they determine the final shape. General constraints for the optimization routine arise from the demand that the individual lenses must not be in contact, except for the intermediate lens' surface in doublets, and that the lens' thickness must be in the range given by the manufacturing process. Furthermore, the angle between incident light and each surface was restricted to angles not too close to the perpendicular in order to ensure that back-reflected intensities were small. The careful choice of a so-called reasonable glass catalogue facilitated the practical aspects of manufacturing. Thus, it was important to use commercially available standard glasses to keep production time and costs low.

Our experience showed that the successive optimization of small subgroups of variables, describing only one lens or a doublet and their positions, enabled better control of the solution than a global optimization, which assumes all parameters (20) to be variables. A solution to a local minimum was thereby more easily avoided. When meaningless, stable local minima occurred, (e.g. total reflecting surfaces), then the optimization process was restarted with another subgroup of variables. Less stable local minima could be overcome by a 'perturbation routine' which added small amounts of noise to the variables. Successive optimization of different subgroups of lenses was repeated, choosing the lens' subgroup contributing the most to the optical errors for the next optimization process. This following subgroup was determined by the aid of the partial Seidel coefficients describing chromatic and spherical errors, astigmatism, coma and field curvature. For the most promising designs, the calculated radii of the lenses were replaced by the nearest radii in the production tool catalogue of the manufacturer.

The final design has six lenses (Fig. 4 and Fig. 5). It was designed by first optimizing a system with five lenses for water immersion and a tube-length of 160 mm. Then, a sixth lens was added and the combination was optimized for infinite tube-length keeping the parameters of the other five lenses constant.

The designs were tested theoretically for reflections in the reverse direction using bright-field reflected-light illumination and the laser beam of the vibrometer. For this purpose, a beam parallel to the optical axis in the reverse direction was assumed (from L6 to L1, Fig. 4), traveling through a perfect transmitting system and reflecting 100% at the optical surface under consideration. The area illuminated by the reflection was calculated by taking the intersection of the back-reflected beam with a plane perpendicular to the optical axis at a distance of 300 mm from the reference plane. This distance is an estimation of the distance between the input-aperture of the laser Doppler vibrometer and the reference plane (Fig. 3). The area of the incident beam as a fraction of the area of the reflected beam was taken as a measure for the percentage of effective back-reflection entering the detector (or camera) from a lens surface (percentages are shown in Fig. 4). This was done successively for all optical surfaces in the system. Due to the antireflection coating ($r < 0.5\%$), multiple reflections were orders of magnitude smaller than the principal reflection and were therefore neglected. Possible designs were finally checked against manufacturing tolerances by theoretically varying lens' positions, lens' thicknesses and radii inside their allowable limits and determining the resultant changes in the theoretical optical properties of the objectives.

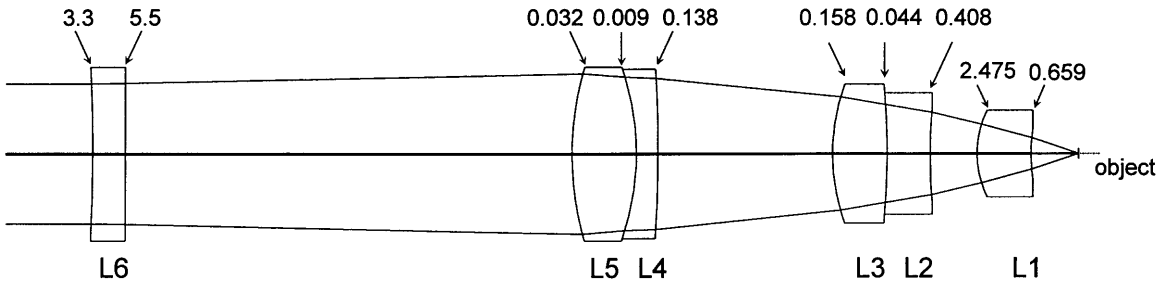

Fig. 4. Percentage of reverse reflections for incident, parallel light from infinity through a pupil with radius 3.21 mm located 47.0 mm from the reference plane at the object. Reflected intensities are given in percent of the initial intensity at a distance of 300 mm from the reference plane. This distance is approximately the position of the entrance pupil of the laser Doppler vibrometer from the object.

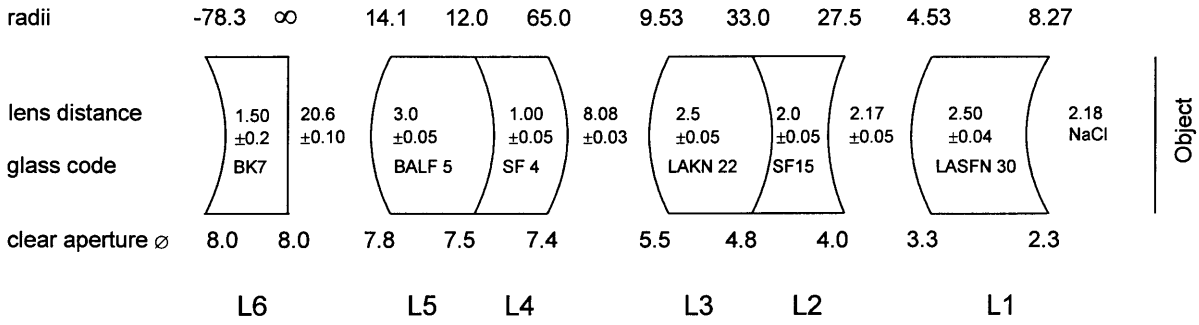

Fig. 5. Lens configuration for the water-immersion objective $\times 25/\infty$ with a working distance of 2.180 mm. A physiological (0.9%) NaCl solution was assumed for the optical properties of the immersion media (refractive index $n = 1.3402$ at 480.0 nm, $n = 1.3372$ at 546.1 nm, $n = 1.3344$ at 632.8 nm). All distances are given in mm. The glass code for each lens is also shown (e.g. BK7, LAKN22).

3.2. Laser vibrometer measurements

Sound-induced vibrations of the cochlear structures were measured using a laser Doppler vibrometer (Polytec OFV 302), coupled coaxially into the light path of an epifluorescence microscope (Leitz Aristomet) with the new objective attached (Fig. 3). Sound was delivered closed-field (Beyer Dynamics DT48) and sound pressures were measured with a 1/4″ probe microphone (Brüel and Kjær 4135). Acoustic stimuli were generated on a digital signal processing PC-card (ELF-31) and consisted of band-limited white noise or clicks. Within each stimulus paradigm, velocity-response waveforms were averaged over multiple presentations and then analyzed by discrete Fourier transformation using an FFT analyzer (Ono Sokki CF6400). Waveforms and spectra were stored on disk for later off-line analysis. All experiments were carried out in a soundproof chamber (Mini S/S, Industrial Acoustics Company Niederkruchen, Germany).

3.3. Surgical procedure

Pigmented guinea pigs (250–400 g) of both sexes showing an intact Preyer reflex (Preyer, 1900) were anaesthetized with Ketanest (120 mg/kg) and Rompun (12 mg/kg). Supplementary doses were administered every hour. ECG was monitored throughout the experiment and the rectal temperature was maintained at 38.5 ± 0.5°C using a thermostatically-controlled heating blanket. Animals were tracheotomized and artificially ventilated with carbogen or room air. A silver wire was placed on the bony promontory near the round window to record gross cochlear potentials. The apical end of the cochlea was exposed ventrally, leaving the internal carotid intact (Weber et al., 1995). To prevent fluid from entering the middle-ear cavity, a rubber cone was fixed with Histoacryl around the apical circumference of the cochlea. Artificial perilymph was then placed on the apical end of the cochlea to allow use of the immersion objective. A small opening in scala vestibuli in the fourth turn of the cochlea was made to allow optical access to the hair cells, tectorial membrane and Hensen cells. Animals were paralyzed with alcuronium chloride (0.1 mg) just before beginning vibration measurements, in order to suppress contraction of the middle-ear muscles. Animal experiments were approved by the Committee for Animal Experiments of the regional council (Regierungspräsidium) of Tübingen.

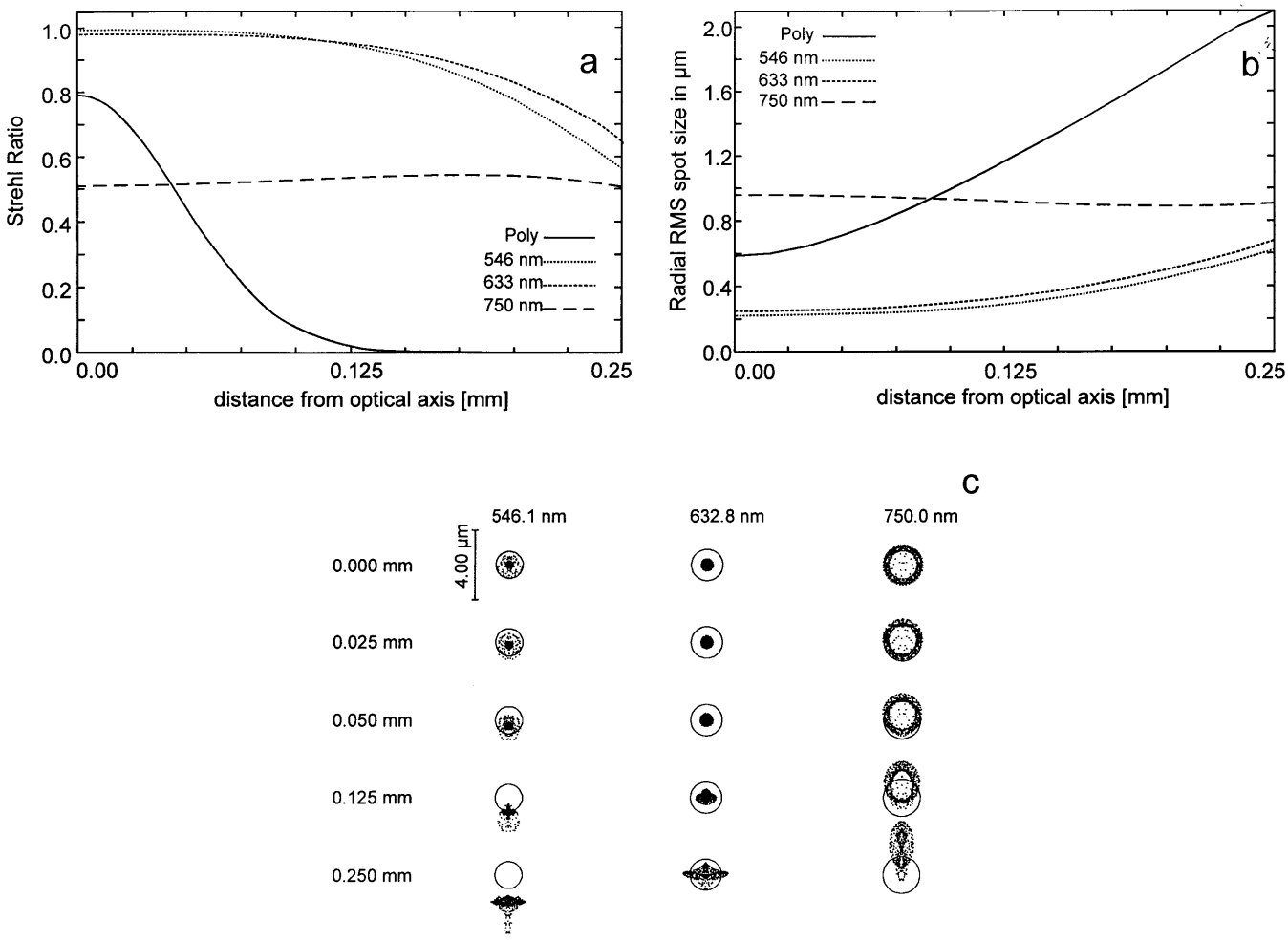

Fig. 6. Performance parameters for the two optimized wavelengths (546.1 and 632.8 nm) and a wavelength around the limit of the visual range (750 nm). The polychromatic line (Poly) includes $\lambda = 750$ nm with equal weight. The object plane (working distance) is 2.180 mm from the front lens. a) Theoretical Strehl ratio versus distance from the optical axis. A broad curve indicates good resolution over a wide optical field. b) Spot size versus distance from the optical axis. A small spot size indicates small spread of the beam. c) Theoretical spot diagrams for several distances from the optical axis. The circles depict the Airy disks, giving the first minimum in the diffraction pattern, which is equivalent to Rayleigh's criterion for resolution. They have radii of 0.780 μm (546.1 nm), 0.904 μm (632.8 nm) and 1.071 μm (750.0 nm). The spot diagrams were calculated using geometric ray-tracing (see text).

4. Results

4.1. Calculated optical performance

Fig. 4 shows the final lens configuration for the objective. The calculation of the reflections (percentages above the lens diagram) showed that only the back-surface of the front lens (L1: 2.5%) and both surfaces of the last plano-convex lens (L6: 3.3%, 5.5%) would contribute reflections in the range of a few percent (if a 100% reflecting surface is assumed). For the quality of the broadband coating specified by the manufacturer ($r < 0.3\%$), this would result in a relative reflected intensity of no more than 0.03%. This reflection is sufficiently low to allow a good view in bright-field reflected-light illumination. In the case of the laser beam from the vibrometer, this fraction is even one or two orders of magnitude lower than that for the bright-field illumination because of a much smaller laser beam diameter than assumed in the calculation (approximately 1.0 mm as opposed to 6.4 mm). A further reduction of reflections would have been possible for selected wavelengths, (e.g. the laser wavelength), but this was thought to be unnecessary.

Initially we began to optimize the achromatic design at blue (480.0 nm) and red (632.8 nm) wavelengths and obtained some promising results. At a later stage we decided to optimize for green (546.1 nm) and red (632.8 nm) because of the spectral characteristics of our CCD camera (Hamamatsu C2400), which is more sensitive for longer wavelengths in the visual range. With this choice, it was possible to achieve a higher performance, (e.g. spot size and Strehl ratio) at the laser wavelength. We also hoped to find a design which could be ex-

tended to the near infra-red, having in mind differential interference contrast (DIC) visualization for patch-clamp recordings (Stuart et al., 1993), but ultimately did not optimize for infra-red. We were able to develop a highly optimized system by restriction to a more limited range. Nevertheless, the final design worked well at infra-red wavelengths, as will be demonstrated later in the paper.

Fig. 5 shows the final design. This system exhibits a resolution for the two wavelengths of optimization which is near the theoretical limit over an extended field (radial distance from the optical axis). The area of diffraction limitation ($\sim \varnothing$ 0.4 mm) is much broader than expected, as can be seen from the Strehl ratio (Fig. 6a) and the RMS spot size (Fig. 6b). Even above the highest visible wavelengths (750 nm) the image is of fairly high quality. This should allow the resolution of small objects such as the stereocilia bundles of hair cells, as indicated by the radius of the Airy disks in Fig. 6c. Here, again, it can be seen that the loss of resolution from the center to the border of the field is remarkably small. Objectives with this characteristic are well adapted for use in combination with a video or photographic system. The calculated spot diagrams (Fig. 6c) indicated only minor distortion: a pincushion distortion for green (546.1 nm), and a barrel distortion for the visible range limit (750 nm). The position of the "center of gravity" of the spot is shifted less than 2 μm at the edge of the field depicted in Fig. 6c, so that an accuracy of 1% of the scale in the radial direction can be expected.

In the theoretical spot diagrams it is obvious that the radial symmetry is broken only for field positions far away from the optical axis, where the image is spread out into a comet-shaped flare (called a 'coma' in optics). This is the result of rays passing through the edge portion of the lens being imaged at a different height than those passing through the center portion. A significant coma does not appear for field positions of 0.125 mm or less, indicating that spherical aberration and astigmatism are small in an extended central field.

An indication of the field curvature and axial chromatic aberration is given by the so-called "longitudinal aberration diagram", depicted in Fig. 7. This was constructed by plotting the focus point for parallel rays incident at different heights above the optical axis. It shows: (i) for the corrected wavelengths (546 and 633 nm), the focus point deviates by less than 2 μm due to chromatic errors, and (ii) the field is flat to within 5 μm. This diagram shows an additional interesting feature which was indicated by the symmetric form of the spot diagram in Fig. 6c: the reduced resolution and Strehl ratio at the visible limit (750 nm) is *not* due to spherical aberrations, but is due to the focus being shifted away from the front lens.

With a corrected working distance of approximately 2.186 mm, the objective also produces a diffraction limited image in the near infra-red (Fig. 8a). The achievable resolution in the infra-red band from 750 to 830 nm (790 mm is the center wavelength of a RG9 infra-red bandpass filter) is near the diffraction limit of 1.130 μm given by the radius of the Airy disk at 790 nm (Fig. 8b, Fig. 8b,c). This is satisfactory for various other applications, such as patch-clamp experiments with infra-red differential interference contrast (Stuart et al., 1993).

4.2. Mechanical design and construction

The final design, shown in Fig. 5, consisted of two single lenses and two cemented doublets. There is also an additional circular light baffle ($\varnothing$ 7.0 mm) on the negative radius side of the last lens (L6) which is not shown in Fig. 5. All glasses are standard types requiring no special grinding or polishing techniques, thus keeping manufacturing time and costs low. The design is insensitive to normal tolerances, given in Fig. 5, thus facilitating fabrication and mounting. The material of the front lens and the anti-reflection coating is sufficiently stable in salt solutions, weak acids and organic solvents and contains no poisonous heavy metals. The front lens is mounted water-tight in the outer housing and sealed with Araldite. Particular attention was given to the mount design to avoid stray light (individual lens' mountings and inner surfaces are blackened). The housing is burnished to prevent accidental laser-light reflections and corrosion of the brass. Because of the different free apertures of the front lens the front lens was given a conical shape and was mounted only at its

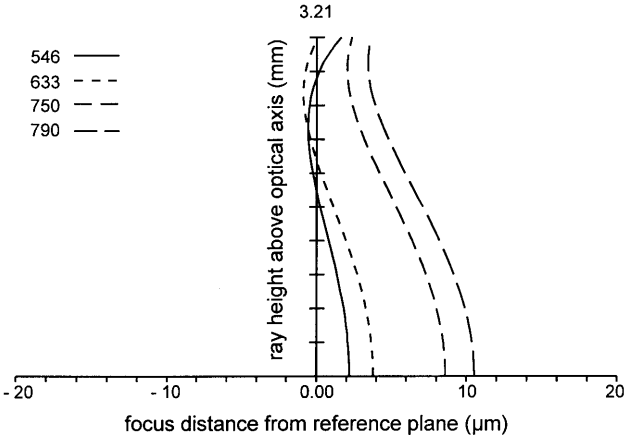

Fig. 7. Longitudinal aberration for wavelengths in the visual and infra-red ranges, showing the height of the ray above the optical axis as a function of the distance of the focus from the reference plane, located 2.180 mm in front of lens L1. The maximum ray height of 3.21 mm is the free aperture of the objective for parallel incident light.

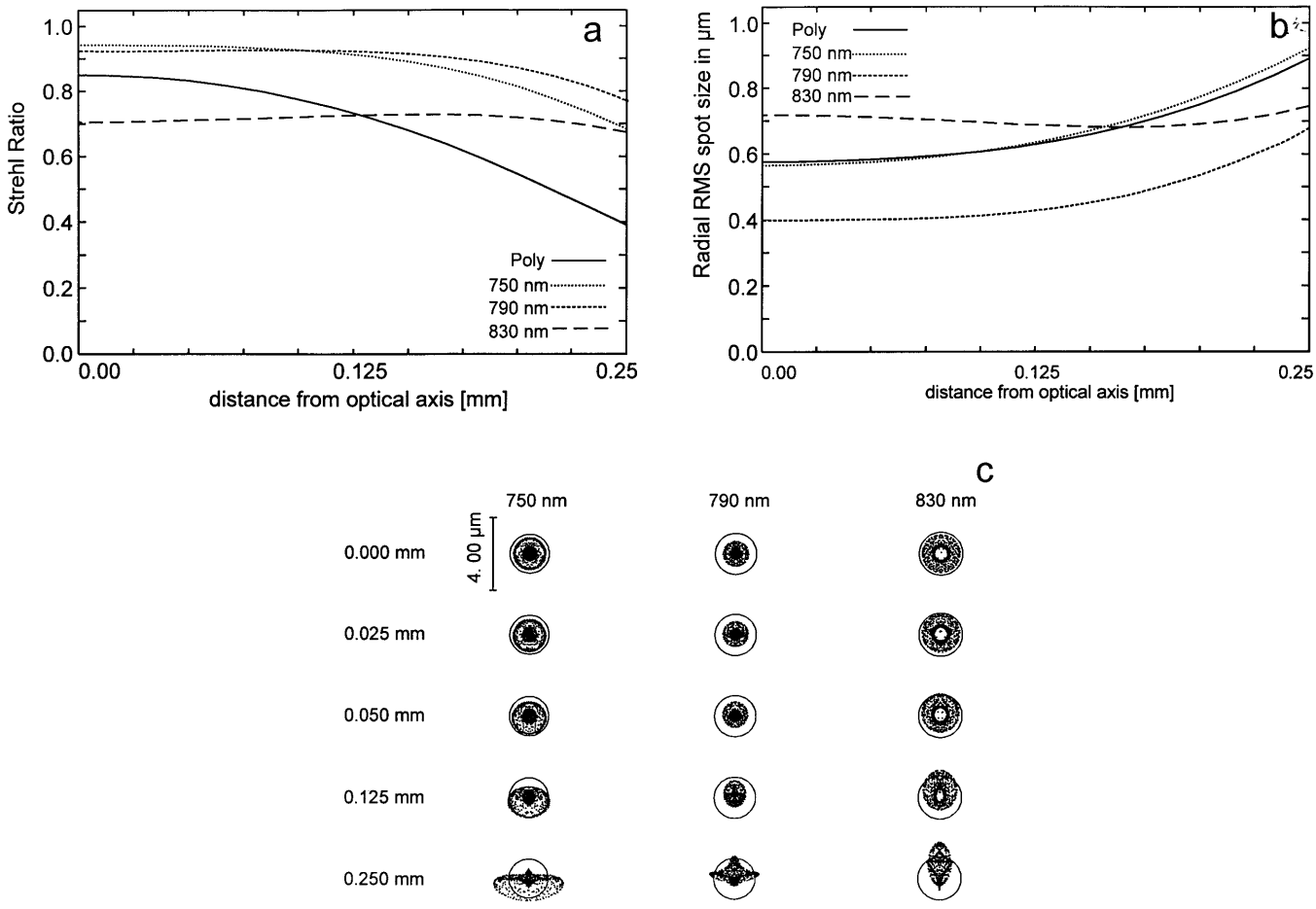

Fig. 8. Performance parameters for the infra-red band around the maximum transmission wavelength of a RG9 filter (790 nm). The object plane (working distance) is 2.186 mm from the front lens and the wavelengths are now 750, 790, and 830 nm. The Airy disk radii are 1.071 μm (750 nm), 1.130 μm (790 nm), and 1.187 μm (830 nm).

rear end, thereby reducing the front lens' diameter to 2.4 mm. A technical drawing of the objective is given in Fig. 9. Lateral surfaces of the cone were varnished black to avoid light scattering. The objective has an overall length of 43 mm with an outer diameter of 11.8 mm and a conical angle of 22°. The thread is a standard 0.797″x36 T.P.I Royal Microscopic Society mounting thread.

4.3. Laserinterferometric performance test

To test the theoretical predictions and the sensitivity under in vivo conditions, vibration measurements were made of cochlear structures in the apical turn of the cochlea using a laser Doppler vibrometer (Fig. 3). When the apical end of the cochlea was exposed ventrally it was always possible to discern the relevant structures optically. The image quality was highly satisfactory in a broad field, readily allowing visual orientation within the cochlea. Cellular structures of the organ of Corti could be distinguished: Hensen cells, the tunnel of Corti and both the apical surface and the nuclei of inner and outer hair cells. Contrast in the visual and video images was good, indicating that reflections were minor. Only faint interference fringes were visible in the laser illumination. Comparison with other water-immersion objectives, (e.g. Olympus WPlan 20x/0.4 W 160/ –) showed that the fringing phenomenon is common. Careful adjustment of the beam of the laser vibrometer reduced the intensity of the reflected light to values near the detection limit. This is approximately one or two orders of magnitude smaller than intensities reflected from the cellular structures in the cochlea.

The velocity of cellular structures was measured in response to white noise and clicks of low and intermediate sound pressure levels. Fig. 10 compares the performance of our objective with that of a commercially available objective. The velocity of a Hensen cell in vitro was measured in response to white noise with an intensity of 66 ± 2 dB SPL per spectral point. Measurements were made without an artificial reflector on the Hensen cell. Near identical results were achieved with both objectives, in spite of the larger numerical aperture of the commercially available objective.

Hensen cells are relatively good reflectors due to lipid droplets inside their soma, having a reflectivity of 0.02–0.039% (Khanna et al., 1989). The reflectivity of outer hair cells compared with Hensen cells is much lower, and ranges from 0.0039–0.017%. Fig. 11 shows the velocity response to clicks (55 ± 2 dB SPL per spectral point) measured directly on the apical surface of an outer hair cell in vivo. This result shows that even in this case artificial reflectors are not required with our objective. The observed spot size of the laser was estimated to be less than 3 μm, as determined from the known diameters of outer hair cells (9–10 μm). In contrast to some commercially available water-immersion objectives, when switching from bright-light illumi-

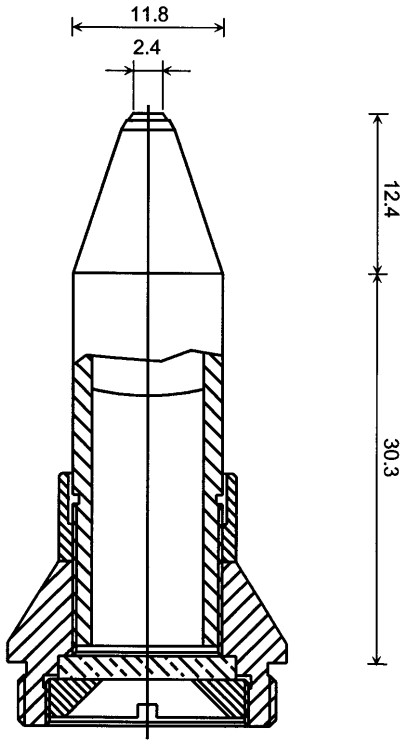

Fig. 9. Technical drawing of the water-immersion objective with its narrow tip (∅ 2.4 mm) and thin body. All dimensions are given in millimeters.

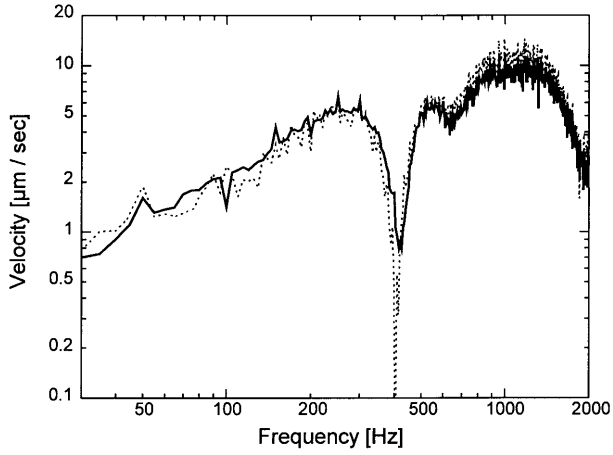

Fig. 10. Comparison of velocity responses measured using our objective $25 \times /0.45$ W (broken line) and a Zeiss Achroplan $40 \times /0.75$ WPh2 (full line). Measurements were made in vitro from a Hensen cell in response to white-noise (66 ± 2 dB SPL per spectral point, 100 averages).

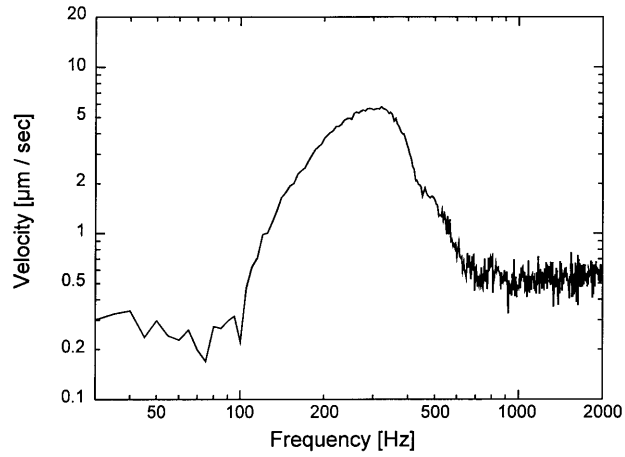

Fig. 11. Velocity amplitude of the apical surface of an in vivo outer hair cell measured using our objective. Click stimuli of 55 ± 2 dB SPL and 200 averages.

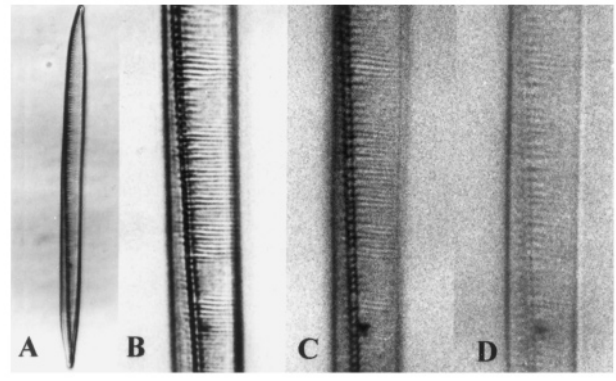

Fig. 12. Resolution tests using a diatom, *Nitzschia spectabilis*. A) Entire structure using the Zeiss Achroplan $20 \times /0.5$ WPh2: Details with B) Zeiss Achroplan $20 \times /0.50$ WPh2, C) our custom-built objective $25 \times /0.45$, D) Nikon MPlan $20 \times /0.35$ SLWD.

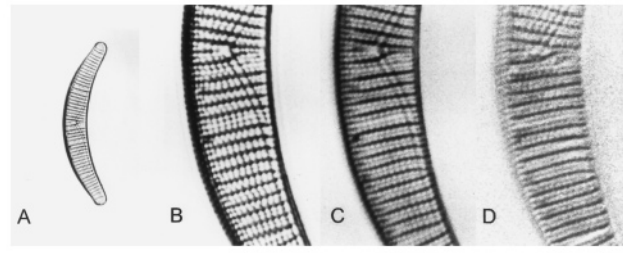

Fig. 13. Resolution tests using a diatom, *Epithemia turgida*. A) Entire structure using the Zeiss Achroplan $20 \times /0.5$ WPh2: Details with B) Zeiss Achroplan $20 \times /0.50$ WPh2, C) our custom-built objective $25 \times /0.45$, D) Nikon MPlan $20 \times /0.35$ SLWD.

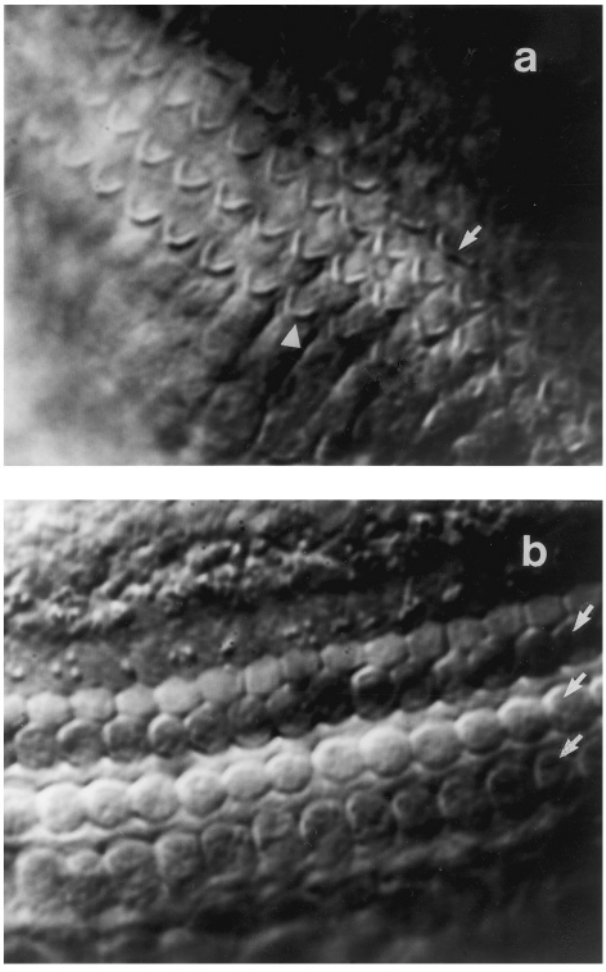

Fig. 14. Images of an organ of Corti in culture (rat, postnatal day 6) obtained with a differential interference contrast microscope in the near infra-red range (RG9 filter) using our objective. a) Bundles of stereocilia of inner hair cells (arrow) and outer hair cells (arrowhead). b) Image section in the organ of Corti, parallel to the reticular lamina through the three rows of outer hair cells (arrows). Computer processing of the images has not been used, except for averaging (16 ×) to reduce noise.

nation to the laser it was not necessary to refocus, indicating that the visual plane of highest resolution is identical to the focal plane of the laser wavelength.

4.3.2 Visual-range microscopy performance test

Although the calculated optical performance of the objective proved sufficient for our purposes, the true resolution of the objective was of interest. Most of the parameters which were used to improve and select different designs were readily calculated with ray tracing techniques, but they cannot be determined experimentally with standard equipment. The necessary devices are not always available even for an optical laboratory, so we decided to perform the resolution tests with standard test objects used in light microscopy. Microscopic images of edges or chrome grids have the advantage that theoretical measures describing resolution, such as the modulation transfer function, are easily calculated from them. However, to obtain reproducible (digitized) images, further basic technical requirements must be fulfilled (e.g. sufficient linearity and resolution of the camera system). An alternative method is to use diatoms as test objects; these are naturally occurring high-contrast, grid-like structures of different sizes. Their use is standard for testing optical resolution (Klosevych, 1989), providing a reproducible and intuitive impression of the optical performance because of their broad variety of fixed-sized internal structures. Fig. 12A shows *Nitzschia spectabilis*, a diatom suggested for numerical apertures between 0.45 and 0.65 (Husted, 1949). The images shown in Fig. 12B–D are details of the same structure obtained with different objectives, having NA from 0.35 to 0.50. It can be seen in Fig. 12B that the horizontal stripes consisting of rows of small pores can be clearly resolved in their full length from one side to the other using the commercially available objective with NA 0.5. With our objective the stripes are also observable in their full extent but with diminished contrast (Fig. 12C). If the NA is further decreased (Fig. 12D), the stripes cannot be seen in their full length and individual lines cannot be clearly distinguished from each other. This result is confirmed with images of *Epithemia turgida* (Fig. 13), where individual pores in the groups of 2–3 horizontal rows are distinguishable from each other for NA 0.5 (Fig. 13B) and NA 0.45 (Fig. 13C), but not for NA 0.35 (Fig. 13D). The comparison clearly shows that the resolution of our objective is equivalent to a commercially built objective of NA between 0.35 and 0.50.

Here it should be mentioned that all images in Fig. 12 and Fig. 13 were made with bright-field transmitted-light illumination, but the resolution is equivalent to that for reflected light, as in cochlear applications when the observation is made with the eye. This is not necessarily the case when a film or video camera is used because they generally have a more restricted dynamic range than the eye. Therefore, the eye can better cope with the back-reflected light from lenses L6 and L1 (Fig. 4). The dynamic range problem can be circumvented by careful adjustment of the subtracted illumination background in the camera.

4.3.3. Infra-red microscopy performance test

The theoretical predictions indicating a good resolution with the objective in the infra-red range were tested under normal operating conditions. For this purpose we used rat organ of Corti in culture to test the resolution and image quality with a DIC microscope in the near infra-red (RG 9 filter). Fig. 14a shows that surface structures like the w-shaped bundles of stereocilia of outer hair cells (600–800 nm width) can clearly

be resolved, as predicted by the performance parameters in Fig. 8. The image quality within the depth of the preparation is illustrated in Fig. 14b. The image shows a section through the soma of the outer and inner hair cells. The picture demonstrates that the resolution is sufficient for patch-clamp experiments. Compared with available water-immersion objectives, which have better numerical apertures and resolutions by virtue of their size, our objective becomes preferable in cases where the accessibility to the object is limited.

5. Conclusion

The key element to the performance of a microscope is the objective lens system. Both theoretical and experimental results have shown that it is possible to handle the challenges arising from the development of a custom-built objective in a small research laboratory. With modern, powerful optical design programs, optical design problems can be solved on a PC platform. If not already available, initial parameters can be obtained from colleagues in University Engineering Departments, patents or from some manufacturers. Together with the assistance of a lens' designer, the procedure is within the capabilities of the biophysicist or neurophysiologist. In our case, the assistance is available at the University of Stuttgart, but assistance can also be obtained at reasonable cost (typically $2000–3000) from commercial designers. The unexpectedly good infra-red characteristics has given rise to another application: namely an infra-red differential interference contrast (DIC) objective, which can be used for patch-clamp experiments (Stuart et al., 1993). The production costs for ten custom-designed objectives were not much more than the total cost of four commercially available water-immersion objectives. In future, it may be possible to produce even smaller production runs, reducing production costs even further.

Acknowledgements

This work is supported by the Deutsche Forschungsgemeinschaft, Gu 194/3–1 and SFB 307, C10. The authors gratefully acknowledge Heiko Wasmund from Syncotec Wetzlar for helpful discussions and valuable help in the construction and development; Bernd Packroß from Lamtech GmbH, Stuttgart, for assistance in development and introduction to ZEMAX and for critical reading of the manuscript; Joachim Rienitz for supplying the microscope test objects; Ulrich Rexhausen and Henry Haase for the DIC microscopy photographs; Gerhard Frank and Robert Patuzzi for critical reading of the manuscript.

References

Cooper NP, Rhode WS. Nonlinear mechanics at the apex of the guinea-pig cochlea. Hear. Res. 1995;82:225–43.

Cooper NP, Rhode WS. Fast traveling waves, slow traveling waves and their interactions in experimental studies of apical cochlear mechanics. Aud. Neurosci. 1996;2:289–99.

Gummer AW, Hemmert W, Zenner H-P. Resonant tectorial membrane motion in the inner ear: its crucial role in frequency tuning. Proc. Natl. Acad. Sci. USA 1996;93:8727–32.

Hilger, A. Aberration of Optical Systems. Series on Optics and Optoelectronics. WT Welford, Bristol and Philadelphia, 243 pp, 1996.

Husted, F. Das Studium der Testdiatomeen als Einführung in die mikroskopische Praxis, Mikrokosmos 12, 1949.

Khanna, SM, Hao, LF. Vibratory characteristics of the reticular lamina in the apical turn of the cochlea in a living guinea pig. Abstracts of the 19th Midwinter research meeting of the Association for Research in Otolaryngology, 63 pp, 1996.

Khanna SM, Willemin J-F, Ulfendahl M. Measurement of optical reflectivity in cells of the inner ear. Acta Otolaryngol. Suppl. 1989;467:69–75.

Klosevych, S. Principles and practice of microscopy and scientific photography. Microscopical Society of Canada, Toronto, 1989.

Nuttall AL, Dolan DF, Avinash G. Laser Doppler velocimetry of basilar membrane vibration. Hear. Res. 1991;51:203–13.

Preyer, WTh. Die Seele des Kindes. Beobachtungen über die geistige Entwicklung des Menschen in den ersten Lebensjahren. 5th edition, Th. Griebens Verlag, Leipzig, p. 57, 1900.

Ruggero MA, Rich NC. Application of a commercially-manufactured Doppler-shift laser velocimeter to the measurement of basilar-membrane vibration. Hear. Res. 1991;51:215–30.

Smith, WJ. Modern Optical Engineering: the Design of Optical Systems, 2nd ed., McGraw–Hill, New York, 336 pp, 1990.

Stuart GJ, Dodt HU, Sakmann B. Patch-clamp recordings from the soma and dendrites of neurons in brain slices using infrared video microscopy. Pflügers Arch. 1993;423:511–8.

Ulfendahl M, Flock Å, Khanna SM. Isolated cochlea preparation for the study of cochlear micromechanics at the cellular level. Hear. Res. 1989;40:55–64.

Weber A, Maier H, Zenner HP, Gummer AW. Entwicklung eines in vivo Verfahrens zur Untersuchung der Mikromechanik des apikalen Abschnitts der Cochlea. HNO Inform. 1995;4:238.